Bone 66 (2014) 223–231

Contents lists available at ScienceDirect

Bone

journal homepage: www.elsevier.com/locate/bone

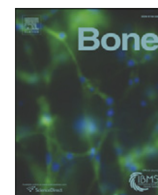

Original Full Length Article

Molecular mechanisms underlying skeletal growth arrest by cutaneous scarring

Jingtao Li [a,b], Chelsey A. Johnson [b,c], Andrew A. Smith [b], Bing Shi [a], John B. Brunski [b], Jill A. Helms [b,*]

[a] Department of Oral and Maxillofacial Surgery, West China Stomatology Hospital, Chengdu 610041, China
[b] Division of Plastic and Reconstructive Surgery, Department of Surgery, Stanford School of Medicine, Stanford CA 94035, USA
[c] College of Medicine, University of Arizona, Tucson, AZ 85719, USA

ARTICLE INFO

Article history:
Received 11 November 2013
Revised 11 March 2014
Accepted 3 June 2014
Available online 14 June 2014

Edited by: Regis O'Keefe

Keywords:
Osteogenesis
Growth inhibition
Finite element model
Scarring
Contracture

ABSTRACT

In pediatric surgeries, cutaneous scarring is frequently accompanied by an arrest in skeletal growth. The molecular mechanisms responsible for this effect are not understood. Here, we investigated the relationship between scar contracture and osteogenesis. An excisional cutaneous wound was made on the tail of neonatal mice. Finite element (FE) modeling of the wound site was used to predict the distribution and magnitude of contractile forces within soft and hard tissues. Morphogenesis of the bony vertebrae was monitored by micro-CT analyses, and vertebral growth plates were interrogated throughout the healing period using assays for cell proliferation, death, differentiation, as well as matrix deposition and remodeling. Wound contracture was grossly evident on post-injury day 7 and accompanying it was a significant shortening in the tail. FE modeling indicated high compressive strains localized to the dorsal portions of the vertebral growth plates and intervertebral disks. These predicted strain distributions corresponded to sites of increased cell death, a cessation in cell proliferation, and a loss in mineralization within the growth plates and IVD. Although cutaneous contracture resolved and skeletal growth rates returned to normal, vertebrae under the cutaneous wound remained significantly shorter than controls. Thus, localized contractile forces generated by scarring led to spatial alterations in cell proliferation, death, and differentiation that inhibited bone growth in a location-dependent manner. Resolution of cutaneous scarring was not accompanied by compensatory bone growth, which left the bony elements permanently truncated. Therefore, targeting early scar reduction is critical to preserving pediatric bone growth after surgery.
© 2014 Elsevier Inc. All rights reserved.

Introduction

In many clinical settings, scarring exerts a negative influence on skeletal growth. For example, a large area of scalding on the back can lead to scoliosis [1], post-burn scarring can cause maxillofacial skeletal deformities [2] and soft tissue scarring can cause multiple types of foot abnormalities [3]. Corrective surgeries to treat pediatric facial defects, such as clefting, also can have a negative influence on skeletal growth [4–7].

In the past, there was speculation that patients with clefting deformities had inherently impaired bone growth [8] but subsequent studies clearly indicate that the growth arrest observed in cleft lip and palate patients is a direct result of the surgical repair [9]. Most cleft lip and palate repairs are performed in the first year of life in order to avoid problems with speech development [10] but the earlier surgical intervention carries with it the potential to more severely impact pediatric skeletal growth [11].

A number of animal models have been developed in an attempt to understand fibrotic scarring [12–16]. To our knowledge, however, there are none that specifically evaluate how scarring adversely impacts skeletal growth. Instead, the majority of studies on wound contraction focus on the etiology of the fibrotic scar itself [17,18], or are performed in vitro [19] and therefore do not recapitulate this skeletal growth arrest problem.

Here, we developed a murine model that recapitulated skeletal growth arrest caused by cutaneous scarring. We used finite element (FE) models to understand the relationship between cutaneous scarring, and to calculate the magnitude and map distribution of contractile forces generated by the scar tissues. We correlated these strain and stress maps with biological data showing how physical forces affected cell death, proliferation, and differentiation and ultimately, how they directly impacted bone growth. In doing so, gained critical insights into how physical and biological events are linked during wound healing.

Methods and materials

Animal surgeries

The Stanford Committee on Animal Research approved all procedures. The tail wound was made on 24 post-natal day 7 (P7) wild type mice. With a ruler, the injury site was marked beginning ~5 mm from

* Corresponding author at: 257 Campus drive, Stanford, CA, 94035.
E-mail address: jhelms@stanford.edu (J.A. Helms).

http://dx.doi.org/10.1016/j.bone.2014.06.007
8756-3282/© 2014 Elsevier Inc. All rights reserved.

the body with a total length of 5 mm. Using a scalpel, a 5-mm long, full-thickness skin excision was made on the dorsal surface of the tail; the tissue was removed gently with forceps. The excision spanned caudal vertebrae 9–12 (CA9–12). Age-matched, intact littermates served as controls.

Finite element modeling

We created a three-dimensional finite element (FE) model in Comsol 4.3b based on the geometry of the wound. We modeled six vertebrae with their associated growth plates (GPs) that were separated by intervertebral disks (IVDs) and surrounded by dermis and epidermis. The mechanical properties of the skin, bone, growth plates, and IVD were assigned based on published reports (Table 1). The area of cutaneous excision was modeled based on the actual size of the wound. The wound region was assigned an initial biaxial tensile stress of magnitude 0.05 MPa in the y- and z-directions. This magnitude of biaxial tensile stress was based on published data [20], which reported a “resting” tension in adult mouse skin = 0.058 MPa and contractile stresses in human skin healing of ~1.5–1.7 MPa. We used a three-step method to arrive at a value of 0.1 MPa for the contractile stress in the healing skin of the mouse. First, we examined the ratio of the resting tension in human skin to the contractile stress in human skin (e.g., [20]). Second, we used that ratio to develop a first-estimate of a contractile stress in mouse skin, given knowledge of the resting tension in mouse skin. Third, we iteratively adjusted the contractile stress used in the FE model until we reached the best match between the predicted vs. measured deflections of the tail.

Histology, immunohistochemistry, and cell activity assays

Mice (N = 8 for each group and each time point) were sacrificed at multiple post-injury time points as indicated. Tail samples were fixed in 4% paraformaldehyde at 4 °C overnight, decalcified in 19% EDTA at room temperature for 3 weeks, and processed for paraffin embedding. Eight-micrometer thick sections were sliced along the longitudinal axis of the tail. Tissue sections closest to the central axis of each specimen were used for analysis. All slides were deparaffinized before staining. Histology was performed using Gomori Trichrome, Movat's Pentachrome, and Safranin O/Fast Green/Hematoxylin staining. For alkaline phosphatase (ALP) staining, slides were pre-incubated for 15 min in NTMT buffer containing 0.1 M Tris buffer, pH 9.0, 0.05 M $MgCl_2$, 0.1 M NaCl, and 0.1% Tween-20. Slides were then stained in ALP solution containing 2 mL NTMT, 10 μl NBT (Roche), and 7.5 μl BCIP (Roche) for 2 h at 37 °C. Tartrate resistant acid phosphatase (TRAP) staining was performed using a leukocyte acid phosphatase kit (Sigma, St. Louis, MO). Ki67 immunohistochemistry was carried out; slides were first immersed in 0.2% Triton for 5 min. Slides were then incubated in Antigen Unmasking Solution (Vector Laboratories, diluted 1:100) at 95 °C for 20 min. After returning to room temperature, slides were immersed in hydrogen peroxide for 5 min then blocked in 5% goat serum for 30 min. Slides were incubated in Ki67 rabbit monoclonal antibody (Thermo Scientific, diluted 1:100) overnight at 4 °C then incubated in biotinylated anti-rabbit antibody for 30 min (Vector Laboratories, diluted 1:200). Slides were then incubated in ABC for 30 min (Vector Laboratories) and developed with DAB (Vector laboratories). For myofibroblast detection, slides were immersed in 0.2% Triton for 5 min, blocked in 5% goat serum for 30 min, then incubated in Vimentin chicken antibody for 90 min (Millipore, diluted 1:500). The slides were then incubated in Alexa Fluor 555 goat anti-chicken antibody (Invitrogen, diluted 1:500) for 30 min, blocked with M.O.M. blocking solution (Vector Laboratories) for 1 h, and immersed in MOM working solution (Vector) for 5 min. The slides were incubated in alpha smooth muscle actin antibody (Sigma, diluted 1:1000) overnight at 4 °C and then mounted with DAPI mounting medium (Vector Laboratories). To detect cell death, TUNEL (In Situ Cell Death Detection Kit, Roche) was performed as described by the manufacturer. Imaging of stained tissue sections was performed with a Leica DM 5000B fluorescent microscope. Adobe Photoshop and Image J software were used to quantify Ki67 and TUNEL positive cells from three slides of each specimen as described [29].

Table 1
Mechanical properties of tissues constructed in the finite element model.

Tissue	Young's elastic modulus (E), Poisson's ratio (ν)	References
Vertebral body (trabecular bone)	E = 100 MPa, ν = 0.2	[21] [22]
Skin	E = 0.1 MPa, ν = 0.45	[23] [24]
Growth plate	E = 0.35 MPa, ν = 0.3	[25] [26,27]
Intervertebral disk	E = 0.5, ν = 0.49	[28]

Cell quantification

Regions of interest (ROI) within the wound bed were photographed (with a minimum of 6 images per sample, and 6 separate samples being used). In the cases of TUNEL and Ki67, the number of positively stained cells was counted. ROI included the IVD and the proliferating zone (e.g., see dotted lines, Fig. 4A).

To determine the height of the hypertrophic zone, we followed established protocols [30,31]. Briefly, a ROI was chosen (e.g., yellow arrows, Figs. 4I,J and 5J,K), and the number of hypertrophic chondrocytes in each column was directly counted from the photographed 8 μm tissue sections using manual selection. The maximal height of each chondrocyte was measured in the direction parallel to the direction of growth [30].

Micro-CT scanning and measurement

Micro-CT scanning (Imtek/Siemens MicroCAT II/SPECT system, 50 um resolution) was performed at PID 7, 14, 21, 35, and 49 on 8 injured and 8 control mice. A radiopaque block was placed next to the tail to mark the injury area. Scanning results were transformed into DICOM format and reconstructed in Mimic software version 10.01 for measurement. The total length of the vertebral segment from CA9–12 and the length of each single vertebra from CA5–16 were measured using the same software.

Statistical analyses

In all quantitative experiments, results are expressed as the mean ± SD. Statistical differences between sets of data were determined by using student t-tests in Microsoft Excel.

Results

Modeling skeletal growth arrest caused by wound contraction and scar formation

To investigate how cutaneous scarring leads to skeletal growth arrest in children, we generated similar wounds on the tails of post-natal day 7 (P7) mice. We chose the tail for two reasons: first, it is a site of rapid skeletal growth during early post-natal life (Fig. 1A) and therefore approximates the rapidly growing facial bones of a pediatric cleft population. Second, the fascia separating the underlying skeletal elements and dermis is thin, which is viewed as a risk factor for facial skeletal growth arrest caused by cutaneous scarring [32]. The cutaneous excision on the pup's tail was strictly limited to the epidermis and dermis and did not directly perturb the paravertebral muscle, the underlying bone, or its periosteum (Figs. 1B,C).

Download English Version:

https://daneshyari.com/en/article/5890214

Download Persian Version:

https://daneshyari.com/article/5890214

Daneshyari.com